Supporting information

For the article "Interaction matters: Bottom-up driver interdependencies alter the projected response of phytoplankton communities to climate change"

Miriam Seifert[1,*], Cara Nissen[1], Björn Rost[1,2], Meike Vogt[3], Christoph Völker[1], and Judith Hauck[1]

[1] Alfred-Wegener-Institut Helmholtz-Zentrum für Polar- und Meeresforschung, Am Handelshafen 12, 27570 Bremerhaven, Germany

[2] Universität Bremen, FB2, Leobener Straße, 28359 Bremen, Germany

[3] Institute for Biogeochemistry and Pollutant Dynamics, ETH Zürich, Universitätstrasse 16, 8092 Zürich, Switzerland

[*] *Corresponding author: miriam.seifert@awi.de*

Content:

Text S.1: Model description

The global Regulated Ecosystem Model version 2 (REcoM-2-M) coupled to the Finite Element Sea Ice-Ocean Model (FESOM 1.4, *Schourup-Kristensen et al.*, 2014; *Wang et al.*, 2014) applies a finite element method to solve the primitive hydrostatic equations on an unstructured mesh (*Sidorenko et al.*, 2011; *Wang et al.*, 2014). The marine biogeochemistry is described by the cycling of carbon, nitrogen, silicon, iron, and oxygen (*Hauck et al.*, 2013; *Karakuş et al.*, 2021). Air-sea CO_2 fluxes as well as the 3D carbonate system are computed by the mocsy 2.0 routine (*Orr and Epitalon*, 2015). The ecosystem includes three phytoplankton groups (diatoms, coccolithophores, and small-sized phytoplankton), two zooplankton groups (small, fast-growing zooplankton and slow-growing polar macrozooplankton), and two detritus groups (slow-sinking and fast-sinking particles). Group-specific phytoplankton parameters are listed in Table S.1. The intracellular stoichiometry of phytoplankton (C:N:Chl:Si for diatoms, C:N:Chl:CaCO3 for coccolithophores, and C:N:Chl for small phytoplankton) is varying with environmental conditions. While diatoms and coccolithophores aim to represent phylogenetically distinct groups, the group of small phytoplankton is defined to comprise a wide range of taxa, including, for instance, non-silicifying and non-calcifying haptophytes and green algae. Silicate and calcite production are explicitly performed by diatoms and coccolithophores, respectively.

Biomass changes in each phytoplankton group result from the balance between growth and loss terms. The growth rate GR of phytoplankton group p (diatoms, coccolithophores, or small phytoplankton) is parametrized as a function of its maximum growth rate constant (μ^{max}, Table S.1), the most limiting nutrient (f^N; dissolved inorganic nitrogen, DIN, or dissolved iron, DFe, or, for diatoms, dissolved silicic acid, DSi), temperature (f^T), light (f^L), and the carbonate system (f^{CO2}):

$$\mathrm{GR}_p = \mu_p^{max} \cdot f_p^N \cdot f_p^T \cdot f_p^L \cdot f_p^{CO2}. \tag{S.1}$$

The most limiting nutrient that determines f^N is derived from the limitations l by the individual nutrients, namely dissolved inorganic nitrogen, DIN and dissolved iron, DFe (for diatoms additionally dissolved silicic acid, DSi):

$$f_p^N = \min(l_p^{DIN}, l_p^{DFe}). \tag{S.2}$$

Limitations by DIN and DSi depend on the group-specific half-saturation constants (k^{DIN} and k^{DSi}, Table S.1) as well as the intracellular nitrogen-to-carbon or silicon-to-carbon ratios, respectively (*Geider et al.*, 1998; *Hauck et al.*, 2013). The limitation by DFe is described by a Michaelis-Menten function that depends on the group-specific half-saturation constants for DFe (k^{DFe}, Table S.1) as well as the concentration of DFe in the water column (*Hauck et al.*, 2013).

The temperature dependence of diatoms and small phytoplankton is described by an Arrhenius function:

$$f^T_{Arrhenius} = \exp\left(-4500 \cdot \left(\frac{1}{T_K} - \frac{1}{T_{K,ref}}\right)\right), \tag{S.3}$$

with T_K being the temperature in K, and $T_{K,ref}$ being the reference temperature of 288.15 K (15°C). The temperature dependence of coccolithophores follows a power function as proposed by *Fielding* (2013):

$$f^T_{cocco} = 0.1419 * T^{0.8151}_{deg}, \tag{S.4}$$

with T_{deg} being the temperature ≥0 in °C. The function is set to a small value (2.23×10^{-16}) at temperatures <0°C. The light function f^L depends on photosynthetically active radiation (PAR) and follows *Geider et al.* (1998):

$$f^L_p = 1 - \exp\left(\frac{-\alpha_p \cdot q^{Chl}_p \cdot \mathrm{PAR}}{\mu^{max}_p \cdot f^N_p \cdot f^T_p}\right), \tag{S.5}$$

with q^{Chl} being the variable chlorophyll-to-carbon ratio and α the group-specific maximum light harvesting efficiency (Table S.1).

The growth dependence on carbonate system parameters f^{CO_2} was developed in *Seifert et al.* (2022) by fitting optimum functions adapted from *Bach et al.* (2015) to a compilation of laboratory data. It accounts for beneficial effects of increasing bicarbonate (HCO^-_3) and $CO_{2(aq)}$ concentrations which are substrates for photosynthesis, and for growth-decreasing acidification effects by the concomitantly decreasing pH:

$$f^{CO_2}_p = \frac{\mathrm{a} \cdot \mathrm{HCO^-_3}}{\mathrm{b} + \mathrm{HCO^-_3}} - \exp(-\mathrm{c} \cdot \mathrm{CO_{2(aq)}}) - \mathrm{d} * 10^{-\mathrm{pH}}. \tag{S.6}$$

Group-specific parameters a, b, c, and d are listed in Table 3. To account for interactive driver effects, parameter d was modified in the present study (Section 2.2.1).

Calcification is performed by coccolithophores and depends on its specific growth rate GR_{cocco}, coccolithophore biomass (C_{cocco}), and a reference particulate inorganic to organic carbon ratio $(PIC{:}POC)^{ref}_{cocco}$ of 1 which is modified by temperature ($f^T_{CaCO_3}$), DIN limitation ($f^N_{CaCO_3}$), and carbonate system sensitivity ($f^{CO_2}_{CaCO_3}$):

$$CaCO_{3\ cocco} = GR_{cocco} \cdot C_{cocco} \cdot (PIC:POC)^{ref}_{cocco} \cdot f^T_{CaCO_3} \cdot f^N_{CaCO_3} \cdot f^{CO2}_{CaCO_3}, \tag{S.7}$$

with

$$f^T_{CaCO_3} = \begin{cases} 0.104 \cdot T_{deg} - 0.108 & \text{if} \quad T_{deg} < 10.6°C \\ 1 & \text{if} \quad T_{deg} \geq 10.6°C \end{cases} \tag{S.8}$$

and

$$f^{N}_{CaCO_3} = \mathrm{x} \cdot \left(\frac{[\mathrm{DIN}]}{[\mathrm{DIN}] + k^{DIN}_{cocco}} + \mathrm{y} \right). \tag{S.9}$$

Temperature T_{deg} is given in °C, and the parameters x and y in $f^{N}_{CaCO_3}$ are –0.31 and 1.31, respectively. Calcification is decreasing at temperatures below 10.6°C, and increasing under DIN limitation. The function of $f^{CO_2}_{CaCO_3}$ is the same as equation S.6, with a = 1.102, b = 42.38, c = 0.7079, and d = $1.343 \,\mathrm{x}\, 10^7$.

The loss rate of phytoplankton biomass is determined by grazing of the two zooplankton groups on the three phytoplankton groups following *Fasham et al.* (1990), as well as aggregation, respiration, and excretion terms. The small zooplankton group grazes preferentially on small phytoplankton and coccolithophores, and the polar macrozooplankton group on diatoms (*Karakuş et al.*, 2021; *Seifert et al.*, 2022). Calcite dissolution depends on the carbonate ion concentration following *Aumont et al.* (2015) as well as dissolution in zooplankton guts, which was set to 50% of ingested calcite to account for calcium carbonate dissolution above the saturation horizon (*Jansen and Wolf-Gladrow*, 2001; *Sulpis et al.*, 2021).

Text S.2: Sensitivity of phytoplankton biomass to the parametrization of driver interactions

As a result of the limited database of laboratory experiments, the relative differences between the observed interactive growth rates A2B2 and the theoretical additive growth rates $\mathrm{A2B2_{add}}$, g_{rel}, have a large spread (standard deviations of up to ±34%; Table 2). Hence, the averaged values of g_{rel} for each phytoplankton group are rather an approximation. To test the sensitivity of phytoplankton biomass at present-day conditions to variations of g_{rel}, we computed values for $m_{final,CxT}$ and $m_{final,CxL}$ of each phytoplankton group based on the group and interaction-specific standard deviations given in Table 2. We performed four simulations by using these values in equation 12 (g_{rel} ± standard deviation at present-day and at future conditions). The simulations were analysed after only 19 years of computation (as opposed to the 32 years of the other model simulations in this study). However, as spatially and depth-integrated biomass remain rather stable over the last years of the simulations (less than ±3 Tg C), we are confident that the sensitivity simulations are representative for variabilities in biomass changes from present-day to future conditions. The results show that a variation of g_{rel} by its standard deviations reverses the direction of change for global and southern high latitude diatoms in the simulation in which standard deviations are added to g_{rel} (Figure S.2). For coccolithophores, the direction of change is reversed in all simulations in which standard deviations are subtracted from g_{rel}. Furthermore, changes in the phytoplankton community composition are modified in the sensitivity simulations compared to the actual simulations. For example, a shift of the southern high latitude community towards a lower share of diatoms and a higher share of small phytoplankton (Figure 5) is not observed in the simulation with added standard deviations (Figure S.2).

Text S.3: Comparison with observations

We evaluate the PR_CTRL simulation by comparing modelled environmental drivers with observations on a global scale (Figure S.5). We use observed sea surface temperatures (Figure S.5a) from the World Ocean Atlas 2018 (*Locarnini et al.*, 2019) and observed surface chlorophyll *a* data from the Ocean-Color Climate Change Initiative (OCCCI) between the years 2012 and 2015 (Figure S.5b, *Sathyendranath et al.*, 2019). Modelled surface dissolved inorganic carbon (DIC) and alkalinity (Figure S.5c,d) are compared to data of the Global Ocean Data Analysis Project (GLODAPv2.2016b, *Lauvset et al.*, 2016) that are based on measurements from the years 1972–2013 (normalized to the year 2002 to remove anthropogenic carbon accumulation). Interannual means of mixed-layer depth data between 1961 and 2008 (Figure S.5e,f) were obtained from IFREMER (`https://cerweb.ifremer.fr/deboyer/mld/home.php`, access date: 21 December 2022; computed based on *de Boyer Montégut et al.*, 2004). The comparison reveals that our model correlates well with observed sea surface temperatures (correlation coefficient: 0.99), while differences in the spatial patterns of chlorophyll *a* lead to a correlation coefficient of 0.6 (logarithmic scale) and a root mean square error of 1, which is, however, in the range of other biogeochemistry models (e.g., *Yool et al.*, 2013; *Aumont et al.*, 2015; *Séférian et al.*, 2019; *Stock et al.*, 2020). DIC and alkalinity are generally understimated in the low and overestimated in the high latitudes compared to observations. Finally, the model partly overestimates the winter mixed layer depth, which leads to a correlation coefficient to 0.75 (March) and 0.89 (September), respectively. Data of the PR_INTER simulation are similar (chlorophyll *a*, correlation coefficient >0.99) or the same (all others) than data of the PR_CTRL simulation.

Text S.4: Present-day and future levels of environmental drivers

Present-day mixed layer depths (MLD) vary seasonally and are deepest in March in the northern hemisphere and in September in the southern hemisphere (up to 900 m; Figure S.6a,b). Present-day levels of mixed-layer averaged temperature (Figure S.6d) and PAR (Figure S.6e) show a clear latitudinal gradient from high values (about 30°C and 90 $\mathrm{W\,m^{-1}}$) in the tropics/subtropics to low values in the high latitudes (<4°C and <10 $\mathrm{W\,m^{-1}}$). By contrast, the pattern of mixed-layer $p\mathrm{CO_2}$ (Figure S.6c) is more patchy (between 250 and 500 μatm) and is modfied by a combination of water temperature (lower temperature increases solubility), mixed layer depths ($\mathrm{CO_2}$ concentrations usually increase with depth), ocean circulation (upwelling of $\mathrm{CO_2}$-rich water and downwelling of low-$\mathrm{CO_2}$ water) and seasons (drawdown of $\mathrm{CO_2}$ by primary production; Figure S.6). A comparison of present-day levels of surface temperature, chlorophyll *a*, dissolved inorganic carbon, alkalinity, as well as mixed layer depths with observations is displayed and described in Text S.3 and Figure S.5. The future mixed layer depth changes on average globally by about ±20 m, and locally even by up to ±500 m compared to present-day (Figure S.6f,g). The ML becomes shallower mainly in the

subtropics and temperate zones. In the tropics, shallowing of the ML is small (about 15-30 m) but persists year-round, while changes in the ML in other regions only occur on a seasonal time scale. The ML deepens in the Southern Ocean and in parts of the northern high latitudes. Future levels of mixed-layer pCO_2 depict a year-round global increase by about 550 μatm (Figure S.6h). Future levels of mixed-layer temperature is about 2°C higher than present-day levels (Figure S.6i), with the strongest warming in the northern hemisphere in September (up to 5°C; not shown). Future levels of mixed-layer PAR depict both increasing and decreasing light levels ($\pm 20\,\mathrm{W\,m^{-2}}$) following changes in the mixed layer, with shallower MLD resulting in higher mixed-layer averaged PAR levels (e.g. in the tropics, where the ML becomes shallower year-round) and vice versa (Figure S.6j).

Table S.1: Values of phytoplankton parameters in REcoM-2-M

Parameter	**Description**	**Unit**	**cocco**[a]	**dia**[b]	**sphy**[c]
μ^{max}	Maximum growth rate constant	d^{-1}	2.80	3.50	3.00
k^{DIN}	N half-saturation constant	mmol N m^{-3}	0.90	1.00	0.55
k^{DFe}	Fe half-saturation constant	μmol Fe m^{-3}	0.09	0.12	0.04
k^{DSi}	Si half-saturation constant	mmol Si m^{-3}	–	4.00	–
q_{max}	Maximum N:C ratio	mol N (mol C)$^{-1}$	0.15	0.20	0.20
q_{min}	Minimum N:C ratio	mol N (mol C)$^{-1}$	0.04	0.05	0.05
q_{max}^{Si}	Maximum Si:C ratio	mol Si (mol C)$^{-1}$	–	0.80	–
q_{min}^{Si}	Minimum Si:C ratio	mol Si (mol C)$^{-1}$	–	0.04	–
σ^{DIN}	Maximum N:C uptake ratio	mmol N (mmol C)$^{-1}$	0.20	0.20	0.20
σ^{DSi}	Maximum Si:C uptake ratio	mmol Si (mmol C)$^{-1}$	–	0.20	–
$q_{max}^{Chl:N}$	Maximum Chl:N ratio	mg Chl (mmol N)$^{-1}$	3.50	4.20	3.15
α	Initial slope of photosynthesis-irradiance curve	mmol C (mg Chl)$^{-1}$ (W m^{-2} d)$^{-1}$	0.10	0.19	0.14
τ_{zoo1}	Grazing preferences of first zooplankton group	dimensionless	0.666	0.083	0.25
τ_{zoo2}	Grazing preferences of second zooplankton group	dimensionless	0.5	1.0	0.5
d^{Chl}	Maximum Chl loss rate constant	d^{-1}	0.50	0.50	0.50
η	Maintenance respiration rate constant	d^{-1}	0.01	0.01	0.01

[a] coccolithophores, [b] diatoms, [c] small phytoplankton

Table S.2: Details on laboratory studies included in the parameterization of driver interactions. Table is submitted as a separate file.

See Seifert_et_al_List_lab_studies.xlsx

Table S.3: Present-day (PR) and future (FU) values of CO_2, nutrient, light, and temperature terms, as well as growth and grazing rates for the three phytoplankton groups in the control simulations (PR_CTRL and FU_CTRL, respectively). The columns "% change" indicate the relative changes between present-day and future values. Regions as indicated in Figure 5.

	Diatoms			**Coccolithophores**			**Small phytoplankton**		
Global	PR	FU	% change	PR	FU	% change	PR	FU	% change
CO_2-term	0.993	0.968	–2.4	0.985	0.902	–8.4	0.976	0.930	–4.7
Nutrient term	0.350	0.348	–0.7	0.455	0.479	+5.3	0.541	0.550	+1.7
Light term	0.142	0.137	–3.4	0.142	0.120	–15.7	0.091	0.084	–8.4
Temperature term	1.176	1.292	+9.9	1.328	1.450	+9.2	1.176	1.292	+9.9
Growth rate (d^{-1})	0.064	0.062	–2.8	0.051	0.049	–3.1	0.077	0.074	–4.1
Grazing rate ($PgC\ d^{-1}$)	2.40	2.09	–12.8	0.26	0.24	–9.6	4.34	3.75	–13.7
Northern high latitudes	PR	FU	% change	PR	FU	% change	PR	FU	% change
CO_2-term	0.977	0.951	–2.7	0.975	0.883	–9.4	0.981	0.912	–7.0
Nutrient term	0.592	0.572	–3.4	0.705	0.721	+2.3	0.782	0.786	+0.4
Light term	0.094	0.096	+2.1	0.172	0.123	–28.6	0.063	0.060	–4.5
Temperature term	0.745	0.842	+13.0	0.772	0.932	+20.9	0.745	0.842	+13.0
Growth rate (d^{-1})	0.074	0.075	+2.2	0.047	0.046	–0.8	0.075	0.075	+0.8
Grazing rate ($PgC\ d^{-1}$)	0.54	0.73	+34.0	0.02	0.03	+46.4	0.52	0.56	+6.7
Tropics/subtropics	PR	FU	% change	PR	FU	% change	PR	FU	% change
CO_2-term	0.995	0.972	–2.4	0.984	0.907	–7.8	0.961	0.935	–2.7
Nutrient term	0.276	0.288	+4.4	0.392	0.426	+8.7	0.461	0.476	+3.2
Light term	0.164	0.156	–4.7	0.103	0.098	–4.9	0.101	0.092	–9.2
Temperature term	1.480	1.612	+9.3	1.744	1.853	+6.2	1.480	1.619	+9.3
Growth rate (d^{-1})	0.064	0.062	–3.0	0.059	0.056	–4.7	0.083	0.079	–5.0
Grazing rate ($PgC\ d^{-1}$)	1.35	1.00	–25.8	0.22	0.16	–27.1	3.03	2.34	–23.0
Southern high latitudes	PR	FU	% change	PR	FU	% change	PR	FU	% change
CO_2-term	0.999	0.972	–2.6	0.998	0.903	–9.5	1.020	0.934	–8.4
Nutrient term	0.388	0.356	–8.3	0.455	0.457	+0.4	0.597	0.595	–0.3
Light term	0.115	0.113	–1.2	0.228	0.179	–21.7	0.083	0.076	–8.5
Temperature term	0.617	0.684	+10.8	0.546	0.677	+24.0	0.617	0.684	+10.8
Growth rate (d^{-1})	0.056	0.051	–8.3	0.031	0.032	+1.7	0.060	0.057	–6.2
Grazing rate ($PgC\ d^{-1}$)	0.44	0.25	–41.7	0.02	0.05	+90.2	0.75	0.80	+6.8

Table S.4: The same as in Table S.3, but for present-day (PR) and future (FU) values of the interaction simulations (PR_INTER and FU_INTER, respectively).

	Diatoms			**Coccolithophores**			**Small phytoplankton**		
Global	PR	FU	% change	PR	FU	% change	PR	FU	% change
CO_2-term	0.991	0.966	–2.5	0.991	0.929	–6.3	0.973	0.916	–5.9
Nutrient term	0.354	0.363	+2.4	0.454	0.473	+4.2	0.535	0.540	+0.9
Light term	0.139	0.128	–7.9	0.141	0.118	–16.3	0.094	0.089	–5.5
Temperature term	1.176	1.292	+9.9	1.328	1.450	+9.2	1.176	1.292	+9.9
Growth rate (d^{-1})	0.063	0.063	–1.3	0.051	0.050	–3.3	0.078	0.074	–4.2
Grazing rate ($PgC\ d^{-1}$)	2.26	2.12	–6.2	0.27	0.25	–7.1	4.58	3.79	–17.3
Northern high latitudes	PR	FU	% change	PR	FU	% change	PR	FU	% change
CO_2-term	0.978	0.953	–2.6	0.954	0.855	–10.4	0.991	0.922	–6.9
Nutrient term	0.601	0.597	–0.6	0.709	0.723	+2.6	0.775	0.769	–0.7
Light term	0.092	0.088	–4.1	0.169	0.117	–30.8	0.065	0.064	–0.7
Temperature term	0.746	0.843	+13.1	0.772	0.934	+21.0	0.746	0.843	+13.1
Growth rate (d^{-1})	0.073	0.072	–0.6	0.046	0.045	–2.0	0.077	0.078	+1.4
Grazing rate ($PgC\ d^{-1}$)	0.47	0.51	+9.2	0.02	0.04	+98.6	0.55	0.55	+0.6
Tropics/subtropics	PR	FU	% change	PR	FU	% change	PR	FU	% change
CO_2-term	0.992	0.967	–2.5	1.011	0.977	–3.4	0.949	0.900	–5.1
Nutrient term	0.279	0.297	+6.2	0.390	0.418	+7.1	0.455	0.468	+2.9
Light term	0.160	0.145	–9.7	0.102	0.095	–6.7	0.104	0.097	–7.0
Temperature term	1.481	1.619	+9.3	1.744	1.853	+6.3	1.481	1.619	+9.3
Growth rate (d^{-1})	0.064	0.063	–1.4	0.060	0.058	–3.8	0.082	0.077	–6.7
Grazing rate ($PgC\ d^{-1}$)	1.33	1.12	–15.5	0.22	0.17	–22.8	3.06	2.21	–27.7
Southern high latitudes	PR	FU	% change	PR	FU	% change	PR	FU	% change
CO_2-term	0.999	0.974	–2.5	0.966	0.850	–12.0	1.035	0.958	–7.5
Nutrient term	0.370	0.382	–2.0	0.452	0.447	–1.0	0.592	0.580	–2.0
Light term	0.113	0.109	–3.4	0.229	0.183	–20.1	0.086	0.083	–3.3
Temperature term	0.617	0.684	+10.9	0.546	0.677	+24.0	0.617	0.684	+10.9
Growth rate (d^{-1})	0.054	0.052	–3.5	0.030	0.029	–3.0	0.065	0.064	–1.0
Grazing rate ($PgC\ d^{-1}$)	0.41	0.40	–2.0	0.02	0.03	+34.4	0.94	0.98	+3.5

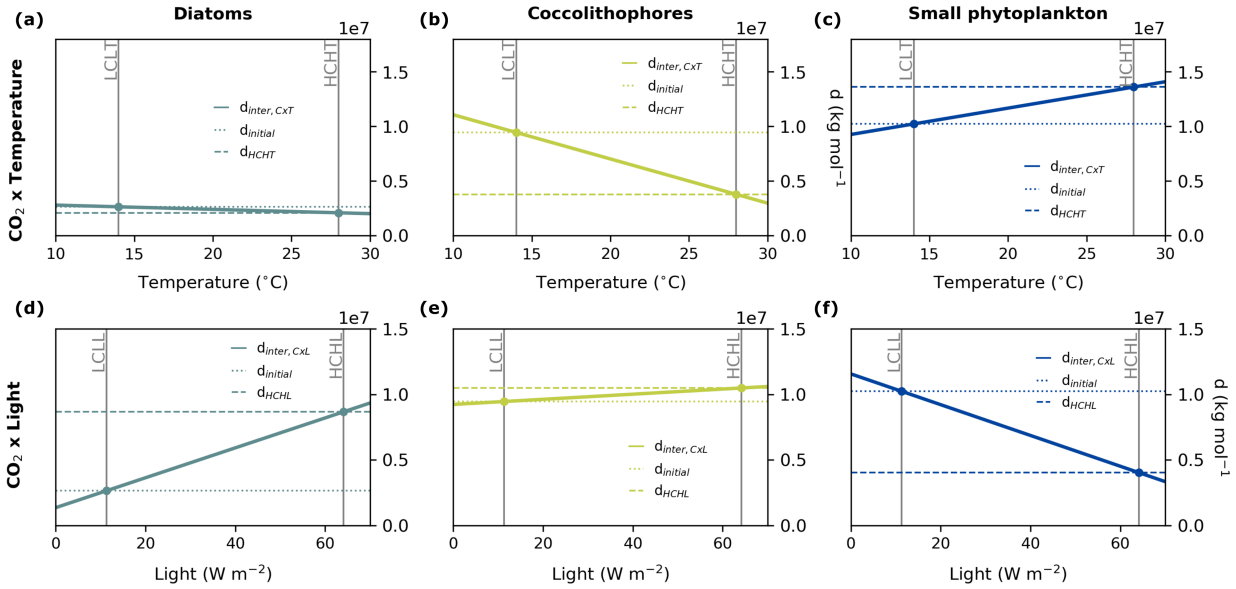

Figure S.1: Illustration of $d_{inter,CxT}$ (a, b, c) and $d_{inter,CxL}$ (d, e, f) for the three phytoplankton groups in the model (solid lines). Vertical lines indicate low and high temperature and light control levels under low and high CO_2 control levels, respectively. The values of d that intersect with these lines represent $d_{initial}$ (dotted lines) and d_{HCHT} or d_{HCHL}, respectively (dashed lines), which result in growth rates GR^{LCLT} and GR_{inter}^{HCHT} for panels a, b, and c, and GR^{LCLL} and GR_{inter}^{HCHL} for panels d, e, and f (equations 5 and 7).

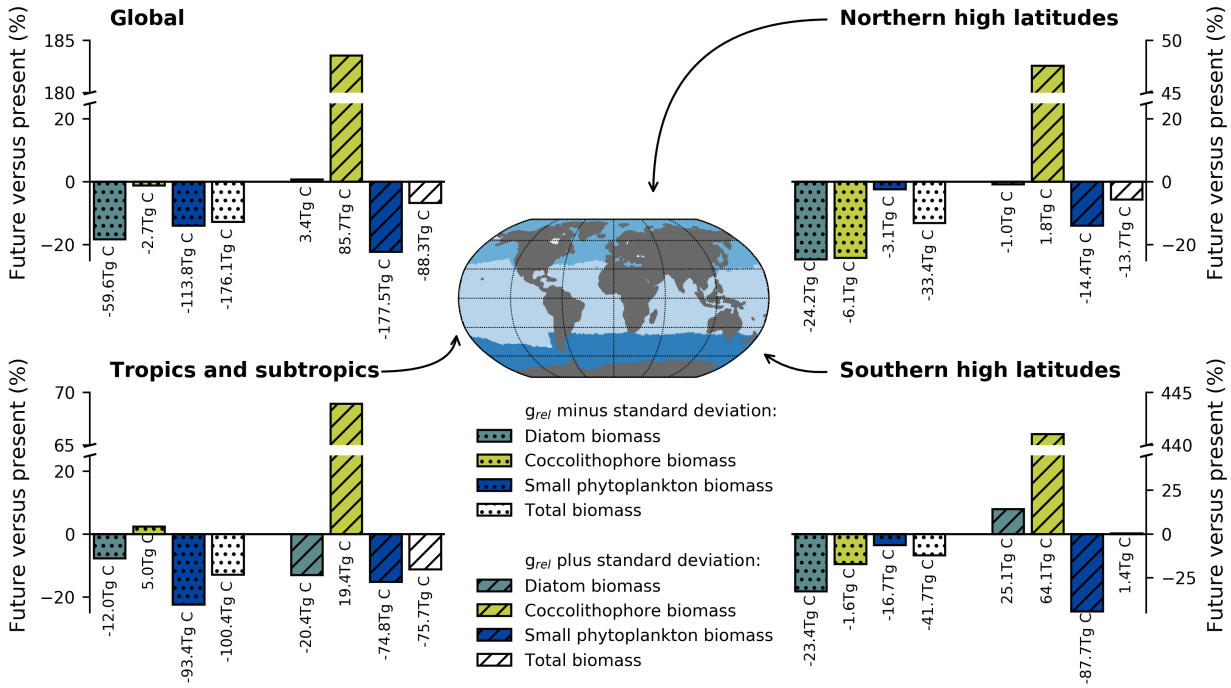

Figure S.2: Relative differences of spatially and depth-integrated phytoplankton biomass between the sensitivity simulations with g_{rel} minus standard deviation at future (FU) and present-day (PR) conditions (FU_CTRL and PR_CTRL; dotted bars) as well as between the sensitivity simulations with g_{rel} plus standard deviation at future and present-day conditions (FU_INTER and PR_INTER; hatched bars) globally, in the northern and southern high latitudes, as well as in the tropics/subtropics. In the sensitivity simulations, values of $m_{final,CxT}$ and $m_{final,CxL}$ are used that are computed based on a reduction of g_{rel} by the standard deviation (SD) of each phytoplankton group and interaction (g_{rel} – SD) and an increase of g_{rel} by the respective standard deviation (g_{rel} + SD) compared to values of g_{rel} in Table 2. Regions as indicated on the map. Total biomass differences are denoted at the respective bars.

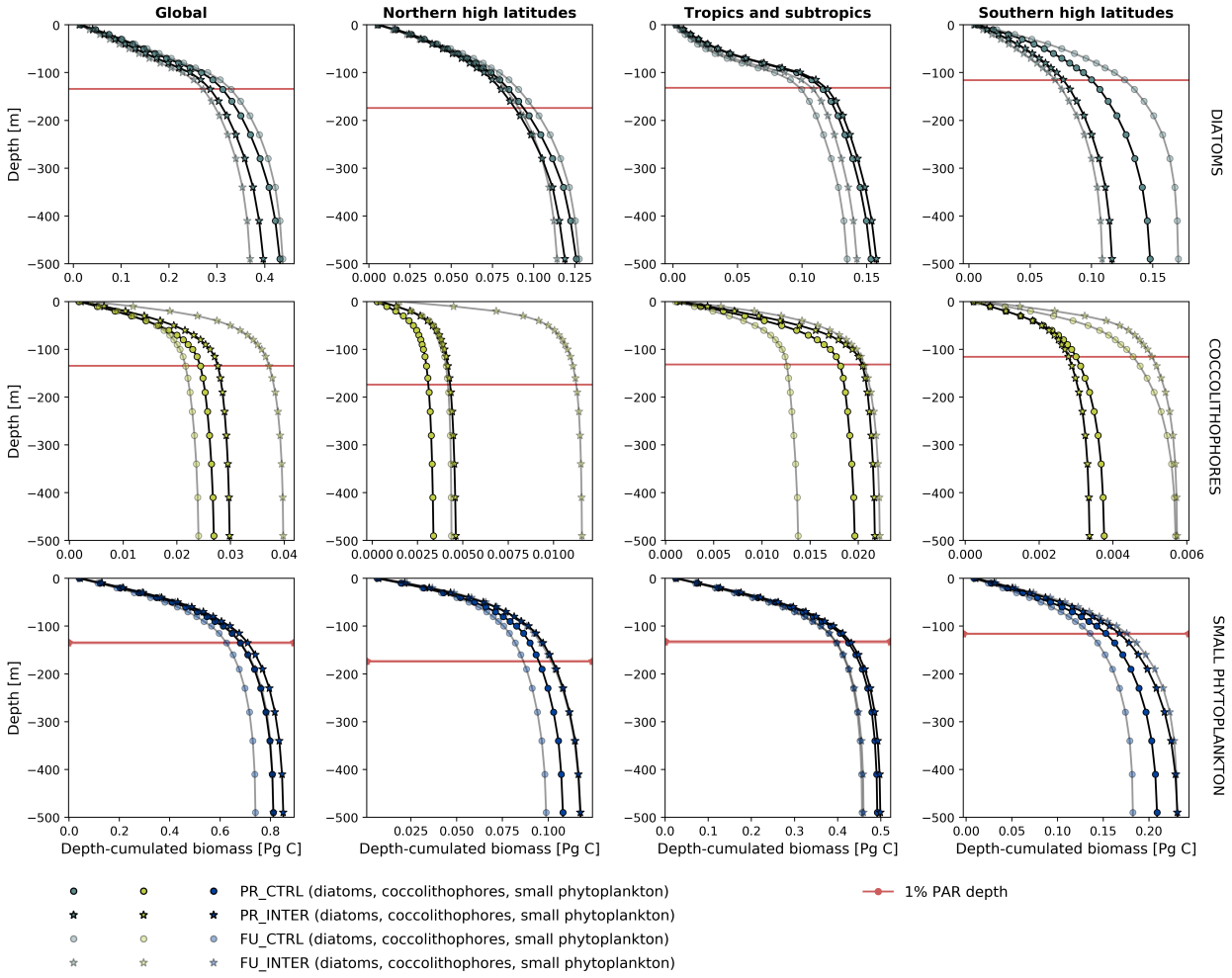

Figure S.3: Phytoplankton biomass cumulated from the surface to depth for the present-day control (PR_CTRL; circles) and interaction (PR_INTER; stars) simulation as well as for the future control (FU_CTRL; circles, pale) and interaction (FU_INTER; stars, pale) simulation. The depth where 1% of surface photosynthetically active radiation (PAR) is reached (bottom of the euphotic depth layer) is indicated by red lines. Because in the annual and spatial mean, the 1% PAR depth varies by only a few meters between the simulations (Figure S.7), we display only one depth per region. The euphotic depth layer contains about 60-80% of the biomass of each phytoplankton group. Regions as indicated in Figure 5.

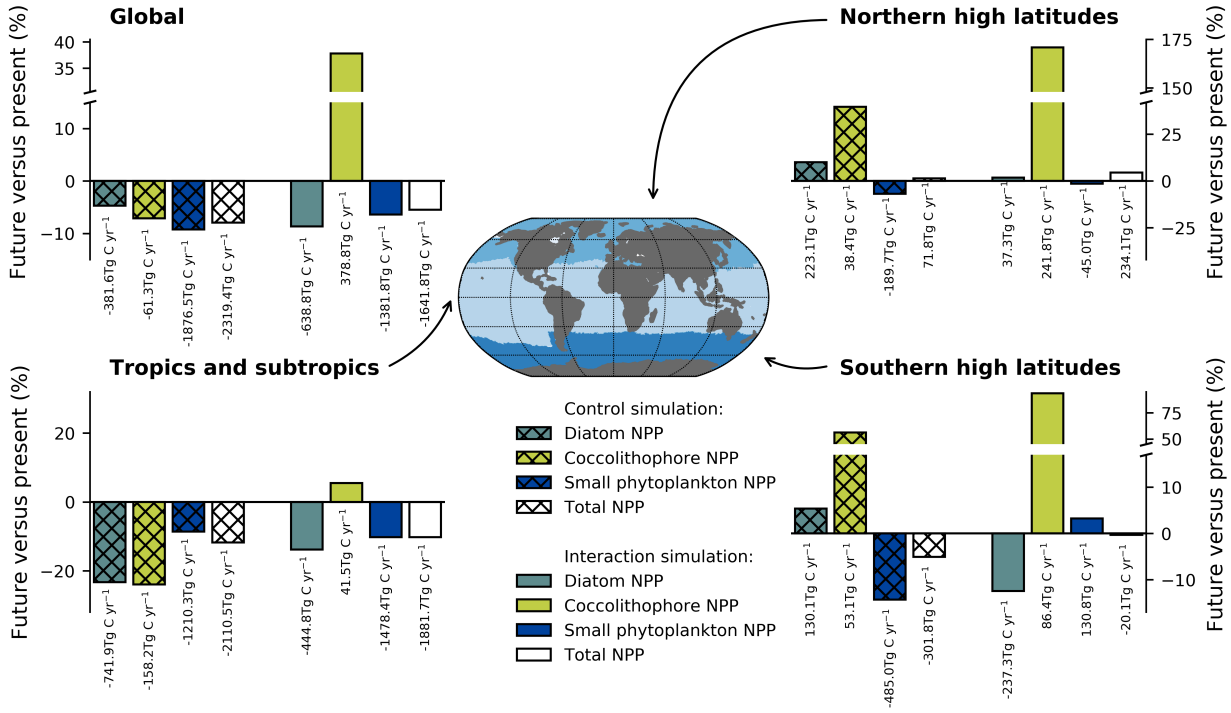

Figure S.4: Relative differences of spatially and depth-integrated phytoplankton net primary production (NPP) between the control (CTRL) simulations at future (FU_CTRL) and present-day (PR_CTRL) conditions (hatched bars) as well as between the interaction simulations (INTER) at future (FU_INTER) and present-day (PR_INTER) conditions (filled bars) globally, in the northern and southern high latitudes, as well as the tropics/subtropics. Regions as indicated on the map. Total NPP differences are denoted at the respective bars.

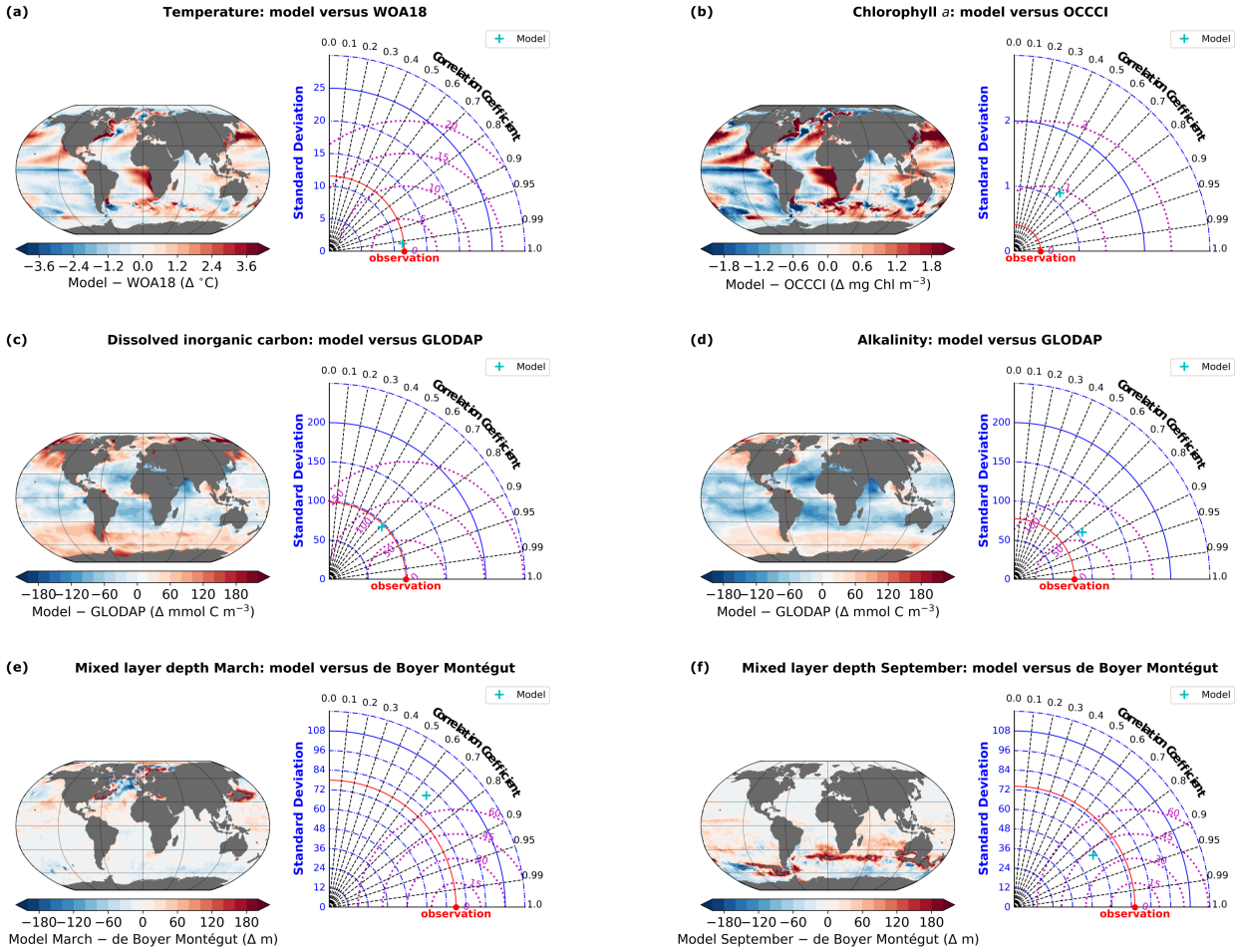

Figure S.5: Comparison of model data with observations displayed as total differences (maps) and in Taylor diagrams. (a) Sea surface temperature, (b) surface chlorophyll *a* concentration, (c) surface dissolved inorganic carbon concentration, (d) surface alkalinity, (e) mixed layer depth in March, and (f) mixed layer depth in September. See Text S.3 for more details on the observational datasets.

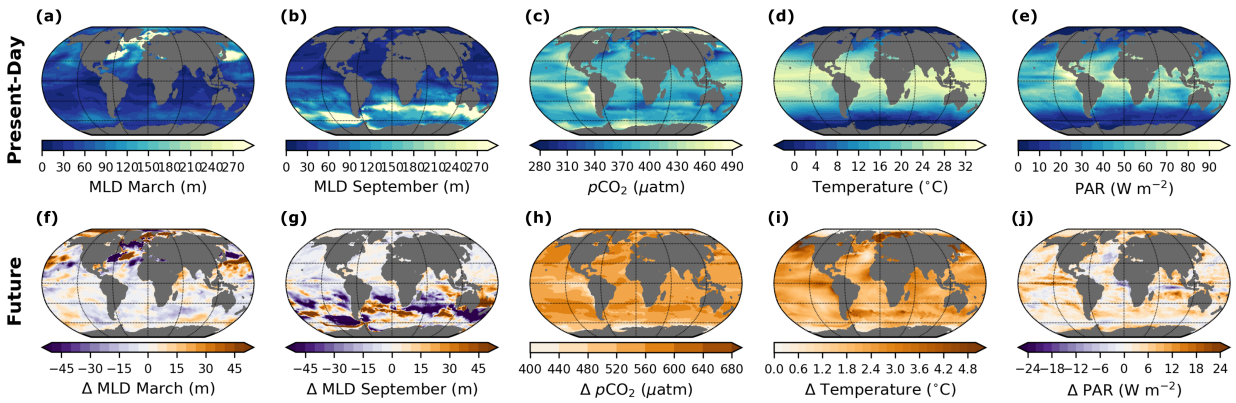

Figure S.6: (a, b, c, d, e) Present-day and (f, g, h, i, j) future (shown as differences to present-day) mixed layer depths in March and September as well as annual means of mixed-layer averaged $p\mathrm{CO}_2$, temperature, and photosynthetically active radiation (PAR). Note that the depth of the mixed layer and, hence, the respective depth layer for $p\mathrm{CO}_2$, temperature, and PAR computations differs between present-day and future simulations.

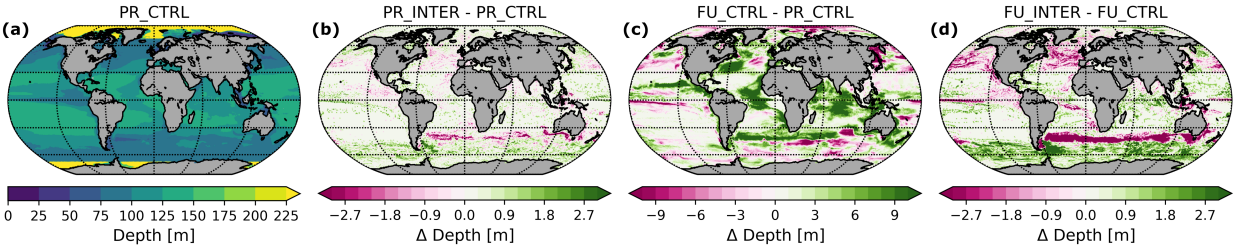

Figure S.7: Annually averaged depths where PAR is 1% of its surface value (i.e. the bottom of the euphotic zone). (a) shows the control simulation at present-day conditions (PR_CTRL), (b) and (c) display the difference between the PR_CTRL simulation and the interaction simulation at present-day conditions (PR_INTER) as well as the control simulation at future conditions (FU_CTRL), respectively. (d) displays the difference between the FU_CTRL and the interaction simulation at future conditions (FU_INTER). Positive values indicate a deepening and negative values a shoaling of the euphotic zone.

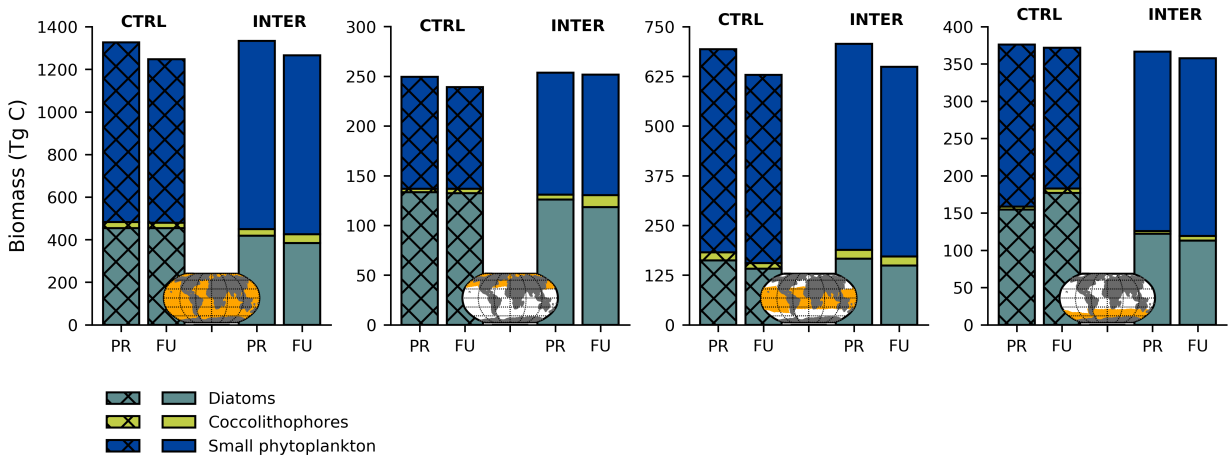

Figure S.8: Integrated biomass of the three phytoplankton groups at present-day (PR) and future (FU) conditions in the control (CTRL: PR_CTRL and FU_CTRL) and interaction (INTER: PR_INTER and FU_INTER) simulations, globally, in the northern and southern high latitudes, as well as the tropics/subtropics. Regions as indicated on the map.

References

Aumont, O., C. Ethé, A. Tagliabue, L. Bopp, and M. Gehlen (2015), PISCES-v2: an ocean biogeochemical model for carbon and ecosystem studies, *Geoscientific Model Development*, *8*(8), 2465–2513, doi:10.5194/gmd-8-2465-2015.

Bach, L. T., U. Riebesell, M. A. Gutowska, L. Federwisch, and K. G. Schulz (2015), A unifying concept of coccolithophore sensitivity to changing carbonate chemistry embedded in an ecological framework, *Progress in Oceanography*, *135*, 125–138, doi:10.1016/j.pocean.2015.04.012.

de Boyer Montégut, C., G. Madec, A. S. Fischer, A. Lazar, and D. Iudicone (2004), Mixed layer depth over the global ocean: An examination of profile data and a profile-based climatology, *Journal of Geophysical Research: Oceans*, *109*(C12), doi:10.1029/2004JC002378.

Fasham, M. J. R., H. W. Ducklow, and S. M. McKelvie (1990), A nitrogen-based model of plankton dynamics in the oceanic mixed layer, *Journal of Marine Research*, *48*(3), 591–639, doi:10.1357/002224090784984678.

Fielding, S. R. (2013), *Emiliania huxleyi* specific growth rate dependence on temperature, *Limnology and Oceanography*, *58*(2), 663–666, doi:10.4319/lo.2013.58.2.0663.

Geider, R. J., H. L. Maclntyre, and T. M. Kana (1998), A dynamic regulatory model of phytoplanktonic acclimation to light, nutrients, and temperature, *Limnology and Oceanography*, *43*(4), 679-694, doi:10.4319/lo.1998.43.4.0679.

Hauck, J., C. Völker, T. Wang, M. Hoppema, M. Losch, and D. A. Wolf-Gladrow (2013), Seasonally different carbon flux changes in the Southern Ocean in response to the southern annular mode, *Global Biogeochemical Cycles*, *27*(4), 1236–1245, doi:10.1002/2013GB004600.

Jansen, H., and D. A. Wolf-Gladrow (2001), Carbonate dissolution in copepod guts: a numerical model, *Marine Ecology Progress Series*, *221*, 199–207, doi:10.3354/meps221199.

Karakuş, O., C. Völker, M. Iversen, W. Hagen, D. W. Gladrow, B. Fach, and J. Hauck (2021), Modeling the impact of macrozooplankton on carbon export production in the Southern Ocean, *Journal of Geophysical Research: Oceans*, *126*(12), e2021JC017315, doi:10.1029/2021JC017315.

Lauvset, S. K., R. M. Key, A. Olsen, S. van Heuven, A. Velo, X. Lin, C. Schirnick, A. Kozyr, T. Tanhua, M. Hoppema, S. Jutterström, R. Steinfeldt, E. Jeansson, M. Ishii, F. F. Perez, T. Suzuki, and S. Watelet (2016), A new global interior ocean mapped climatology: the 1° x 1° GLODAP version 2, *Earth System Science Data*, *8*(2), 325–340, doi:10.5194/essd-8-325-2016.

Locarnini, R. A., A. V. Mishonov, O. K. Baranova, T. P. Boyer, M. M. Zweng, H. E. Garcia, J. R. Reagan, D. Seidov, K. Weathers, C. R. Paver, and I. Smolyar (2019), World Ocean Atlas 2018, Volume 1: Temperature. A. Mishonow, Technical Editor, *Report*, NOAA Atlas NESDIS 81, 52pp.

Orr, J., and J.-M. Epitalon (2015), Improved routines to model the ocean carbonate system: Mocsy 2.0, *Biogeosciences*, *8*, 485–499, doi:10.5194/gmd-8-485-2015.

Sathyendranath, S., R. J. W. Brewin, C. Brockmann, V. Brotas, B. Calton, A. Chuprin, P. Cipollini, A. B. Couto, J. Dingle, R. Doerffer, C. Donlon, M. Dowell, A. Farman, M. Grant, S. Groom, A. Horseman, T. Jackson, H. Krasemann, S. Lavender, V. Martinez-Vicente, C. Mazeran, F. Mélin, T. S. Moore, D. Müller, P. Regner, S. Roy, C. J. Steele, F. Steinmetz, J. Swinton, M. Taberner, A. Thompson, A. Valente, M. Zühlke, V. E. Brando, H. Feng, G. Feldman, B. A. Franz, R. Frouin, R. W. Gould, S. B. Hooker, M. Kahru, S. Kratzer, B. G. Mitchell, F. E. Muller-Karger, H. M. Sosik, K. J. Voss, J. Werdell, and T. Platt (2019), An Ocean-Colour Time Series for Use in Climate Studies: The Experience of the Ocean-Colour Climate Change Initiative (OC-CCI), *Sensors*, *19*(19), doi:10.3390/s19194285.

Schourup-Kristensen, V., D. Sidorenko, D. A. Wolf-Gladrow, and C. Völker (2014), A skill assessment of the biogeochemical model REcoM2 coupled to the Finite Element Sea Ice–Ocean Model (FESOM 1.3), *Geoscientific Model Development*, *7*(6), 2769–2802, doi:10.5194/gmd-7-2769-2014.

Séférian, R., P. Nabat, M. Michou, D. Saint-Martin, A. Voldoire, J. Colin, B. Decharme, C. Delire, S. Berthet, M. Chevallier, S. Sénési, L. Franchisteguy, J. Vial, M. Mallet, E. Joetzjer, O. Geoffroy, J.-F. Guérémy, M.-P. Moine, R. Msadek, A. Ribes, M. Rocher, R. Roehrig, D. Salas-y Mélia, E. Sanchez, L. Terray, S. Valcke, R. Waldman, O. Aumont, L. Bopp, J. Deshayes, C. Éthé, and G. Madec (2019), Evaluation of CNRM Earth System Model, CNRM-ESM2-1: Role of earth system processes in present-day and future climate, *Journal of Advances in Modeling Earth Systems*, *11*(12), 4182–4227, doi:10.1029/2019MS001791.

Seifert, M., C. Nissen, B. Rost, and J. Hauck (2022), Cascading effects augment the direct impact of CO_2 on phytoplankton growth in a biogeochemical model, *Elementa: Science of the Anthropocene*, *10*(1), doi:10.1525/elementa.2021.00104, 00104.

Sidorenko, D., Q. Wang, S. Danilov, and J. Schröter (2011), FESOM under coordinated ocean-ice reference experiment forcing, *Ocean Dynamics*, *61*(7), 881–890, doi:10.1007/s10236-011-0406-7.

Stock, C. A., J. P. Dunne, S. Fan, P. Ginoux, J. John, J. P. Krasting, C. Laufkötter, F. Paulot, and N. Zadeh (2020), Ocean biogeochemistry in GFDL's Earth System Model 4.1 and its response to increasing atmospheric CO_2, *Journal of Advances in Modeling Earth Systems*, *12*(10), e2019MS002043, doi:10.1029/2019MS002043.

Sulpis, O., E. Jeansson, A. Dinauer, S. K. Lauvset, and J. J. Middelburg (2021), Calcium carbonate dissolution patterns in the ocean, *Nature Geoscience*, doi:10.1038/s41561-021-00743-y.

Wang, Q., S. Danilov, D. Sidorenko, R. Timmermann, C. Wekerle, X. Wang, T. Jung, and J. Schröter (2014), The Finite Element Sea Ice-Ocean Model (FESOM) v.1.4: formulation of an ocean general circulation model, *Geoscientific Model Development*, *7*(2), 663–693, doi:10.5194/gmd-7-663-2014.

Yool, A., E. E. Popova, and T. R. Anderson (2013), MEDUSA-2.0: an intermediate complexity biogeochemical model of the marine carbon cycle for climate change and ocean acidification studies, *Geoscientific Model Development*, *6*(5), 1767–1811, doi:10.5194/gmd-6-1767-2013.